



**HAL**  
open science

# New approach for the measurement of gas permeability and porosity accessible to gas in vacuum and under pressure

Hognon Sogbossi, Jérôme Verdier, Stéphane Multon

► **To cite this version:**

Hognon Sogbossi, Jérôme Verdier, Stéphane Multon. New approach for the measurement of gas permeability and porosity accessible to gas in vacuum and under pressure. *Cement and Concrete Composites*, 2019, 103, pp.59-70. 10.1016/j.cemconcomp.2019.04.032 . hal-02310680

**HAL Id: hal-02310680**

**<https://hal.insa-toulouse.fr/hal-02310680>**

Submitted on 10 Oct 2019

**HAL** is a multi-disciplinary open access archive for the deposit and dissemination of scientific research documents, whether they are published or not. The documents may come from teaching and research institutions in France or abroad, or from public or private research centers.

L'archive ouverte pluridisciplinaire **HAL**, est destinée au dépôt et à la diffusion de documents scientifiques de niveau recherche, publiés ou non, émanant des établissements d'enseignement et de recherche français ou étrangers, des laboratoires publics ou privés.

# **New approach for the measurement of gas permeability and porosity accessible to gas in vacuum and under pressure**

Hognon Sogbossi\*, Jérôme Verdier, Stéphane Multon

*LMDC, Université de Toulouse, INSA, UPS, 135 Avenue de Rangueil, 31077 Toulouse cedex 04, France*

\*Corresponding author: Email: [sogbossi@insa-toulouse.fr](mailto:sogbossi@insa-toulouse.fr)

## **Abstract:**

This study proposes new approaches for measuring the gas permeability and the accessible porosity of porous media. Two techniques are used: the usual permeameter, of the Cembureau type (measurement under pressure), and a new technique named a “double-cell” permeameter, based on a vacuum technique. Theoretical and experimental results point out that the apparent permeability measured in vacuum is proportional to the permeability measured under pressure. For a given pressure, the theoretical expression of the coefficients of proportionality leads to a quasi-constant value for a very large range of concrete permeability. A new equation is also proposed to evaluate the accessible porosity from the Time to Reach Steady State (TRSS) recorded during permeability tests. Concordance between the porosity accessible to gas obtained in this way and the porosity measured by the usual technique of hydrostatic weighing is discussed.

## **Keywords:**

Transfer, permeability, porosity, vacuum, laminar flow, Knudsen flow.

## 26 **1 Introduction**

27 The viability of many structures depends on the concrete transport properties [1]–[5], which  
28 can be evaluated using the permeability. This permeability is quantified by the fluid flow  
29 through the porous medium under the effect of a pressure gradient. During permeability tests,  
30 the gas flow is quantified by measuring the volume flow rate through the porous medium in  
31 steady state (SS).

32 In the laboratory, flow measurements for gas permeability calculations are generally made  
33 under pressure with the Cembureau permeameter [6], [7]. This device needs a measurement  
34 cell and the specimen is inaccessible during flow measurements, so it is not easy to combine  
35 the gas permeability measurement with other tests [8]. Moreover, in situ permeability can be  
36 measured under vacuum. So, a new device that operates in low vacuum and is called a  
37 "double-cell" is used in this study. It can be used for example to perform monitoring of air  
38 permeability under a cyclic mechanical load [9].

39 The parameters that influence the gas flow rate and the corresponding permeability can be  
40 associated with the nature of the gas flow in the porous network [10]. In this paper, the term  
41 "flow regime" is used to name the nature of gas flows. The gas flow regime can be continuum  
42 or laminar flow, slip flow, transition flow, or free molecular or Knudsen flow [11]–[14]. Each  
43 flow regime contributes to the total apparent flow rate in a different proportion and the  
44 proportion can differ for measurements under pressure or in vacuum. For a better analysis of  
45 the permeability measurements, it is therefore important to first determine the contribution of  
46 each of the apparent flow modes to the total apparent flow [15]. In this study, the porous  
47 network is analysed using the time to reach steady state (TRSS), apparent permeability, and  
48 porosity. The TRSS is closely related to the characterization of connectivity and pore  
49 tortuosity [9], [16].

50 The transfer properties of concrete are strongly influenced by its connected porosity. The  
51 porosity of concrete is measured in the laboratory by hydrostatic weighing (the method  
52 described in standard NF P18-459 is generally used [6], [17]), by mercury intrusion, by  
53 nitrogen sorption or by water sorption [18]. These methods take quite a time to perform  
54 (generally one to two weeks) depending on the porosity range of the material. During the  
55 measurement of steady-state apparent flow, the TRSS is a function of the porosity, its  
56 connectivity and its fineness. Therefore, an original equation between the TRSS, the  
57 permeability (or flow rate) and the accessible porosity volume is proposed. In this paper, the

58 porosity obtained with this method is compared to the accessible porosity to water obtained  
59 with usual hydrostatic weighing.

60 The first objective of this study is to establish and analyse an experimental database that  
61 compares permeability obtained from air flow measured in vacuum and under pressure. The  
62 second objective is the analysis of transfer properties to determine the characteristic  
63 permeability for an absolute test pressure of 2 bars,  $k_{a2bars}$ , and the intrinsic permeability  $k_i$   
64 using a single value of apparent permeability obtained in vacuum or under pressure. The third  
65 objective concerns a new approach for the calculation of porosity accessible to gas from the  
66 Time to Reach Steady State (TRSS).

## 67 **2 Materials and methods**

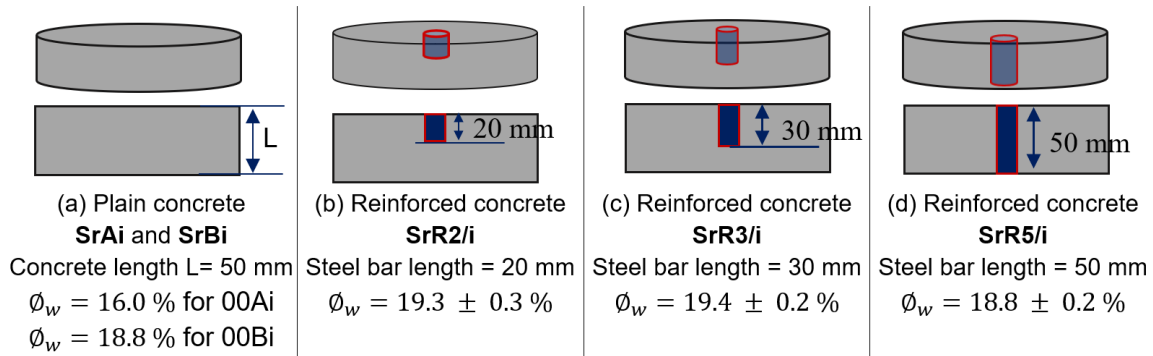
### 68 **2.1 Materials**

69 To compare the permeability obtained in vacuum and under pressure, tests were performed on  
70 two ordinary concretes [9], [19]. Their common characteristics are: the same cement CEM I  
71 52.5 NCE CP2 NF: 320 kg/m<sup>3</sup> and the ratio Gravel / Sand is equal to 0.83. Plain concrete  
72 samples and reinforced samples were tested. Two batches of concrete (A and B) were used for  
73 the plain concrete samples. The ratios water / cement are respectively equal to 0.52 for batch  
74 A and 0.62 for batch B.

75 The concrete of batch A (W/C = 0.52) was used for some plain samples and was  
76 representative of the concrete walls of a power plant and was chosen as part of a national  
77 project [20]. The concrete of batch B (W/C = 0.62) was used for some plain samples and for  
78 reinforced samples.

79 Reinforced samples were used in order to test the limits of validity of the methods proposed in  
80 this paper. It was important to test the measurements and the analysis on samples with  
81 significant defects. Specific reinforced samples with embedded steel bars were used to obtain  
82 samples with preferential percolation paths as explained in [9], [19]. Such percolation paths  
83 have large impact on the apparent permeability of the sample and perhaps on their porosity. It  
84 was thus interesting to test the present method on such samples. Figure 1 presents all the  
85 configurations that were tested during this study and the water porosity of samples for drying  
86 at 105°C.

87 The length of the steel bars lay between 20 and 50 mm and the concrete sample thickness was  
88 50 mm. A steel bar 50 mm long thus crossed the samples completely (Figure 1).



- Sr is the saturation degree; - i identifies the sample: i = 1; 2; 3.

Figure 1: Types and codes of samples [9], [19]

90

## 91 2.2 Methods

### 92 2.2.1 Permeability

93 Flow measurements for gas permeability calculations are usually performed with the  
 94 Cembureau permeameter in laboratory [6], [7]. The standard XP P 18-463 defines one  
 95 permeability value as a standard: the apparent permeability calculated from the flow rate for  
 96 an absolute test pressure of 2 bars. In this study this apparent permeability (designated as  
 97  $k_{a2bars}$ ) is used as the characteristic permeability for a given sample.

98 Performing measurement of permeability under vacuum in laboratory [9] helps to better  
 99 understand the permeability measurement devices which operate under vacuum used on site  
 100 [21]. The gas flow regime differs according to the mechanism controlling the gas transfer  
 101 (under pressure or in vacuum; in particular, the molecular free path is not the same under  
 102 pressure and in low vacuum). This impacts the evaluation of the material permeability. The  
 103 literature provides few information on permeability measurements in vacuum at steady-state  
 104 or on the comparison between permeability measured under pressure and in vacuum. To  
 105 obtain comparative results with the different methods used in the field and in laboratory, it is  
 106 important, first, to acquire valid results for the two techniques on the same sample and then to  
 107 analyse the determination of the permeability in the steady state with the vacuum technique.  
 108 This is one of the objectives of the new “double-cell” device presented here.

### 109 2.2.2 Porosity

110 The accessible porosity is another fundamental property for transfer analysis. Until now, the  
 111 methods used to evaluate this durability indicator have not always been relevant for the  
 112 evaluation of the gas permeability of cementitious materials, as the porosity is often measured  
 113 by a hydrostatic weighing method [6], [17]:

114

$$\phi_w = \frac{M_{air} - M_{dry}}{M_{air} - M_w} \times 100 \quad (\text{Eq. 1})$$

115 where  $\phi_w$  is the water porosity (%),  $M_{air}$  is the mass of the saturated sample measured in air,  
116  $M_w$  is the mass of the saturated sample measured in water and  $M_{dry}$  is the mass of the sample  
117 measured after drying.

118 The global theoretical porosity accessible to gas can be evaluated according to the saturation  
119 degree by:

$$\phi_g = (1 - Sr)\phi_w \quad (\text{Eq. 2})$$

120 where  $\phi_g$  is the porosity accessible to gas (%) and  $Sr$  the saturation degree.

121 Due to the geometry of the pores (connectivity, constrictivity, dead arms), water porosity  
122 cannot be exactly the same as the porosity accessible to gas that participates in the flow  
123 during a permeability test. Consequently, comparisons between experimental data on  
124 porosity-permeability and the predictive calculations performed with different models are  
125 often disappointing [22], [23]. Some researchers have explained these differences by the  
126 approximations made in the description of the microstructure in the models as well as on the  
127 uncertainties regarding the determination of their input quantities.

128 In addition, the measurement of porosity with a hydrostatic weighing method requiring drying  
129 in an oven may be potentially destructive for some specimens. Since the air does not react  
130 with the chemical components of cementitious material, a new approach for gas porosity  
131 calculation based on an air permeability test is proposed in this paper.

## 132 **3 Experimental procedures**

### 133 **3.1 Permeability under pressure**

134 Figure 2 gives an overview of the Cembureau apparatus [7], [24]. The main elements are: an  
135 air supply cylinder fitted with a pressure reducing valve, a precision pressure regulator, a  
136 pressure gauge, the permeability cell, a flow meter and a computer to record the air flow.

137

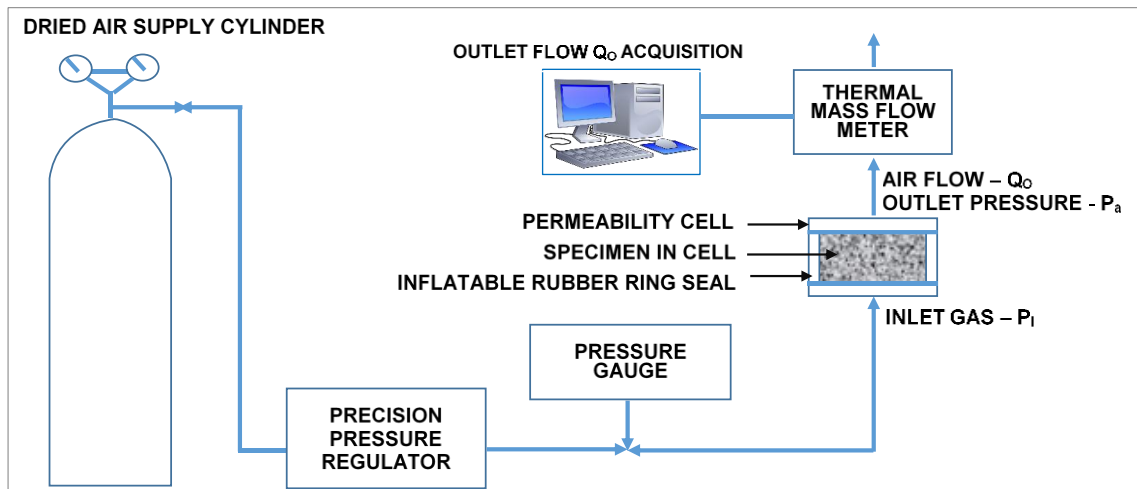


Figure 2: Cembureau device for air flow measurement under pressure

138 **3.2 Permeability under vacuum**

139 Figure 3 gives an overview of the double-cell apparatus to measure permeability under  
 140 vacuum.

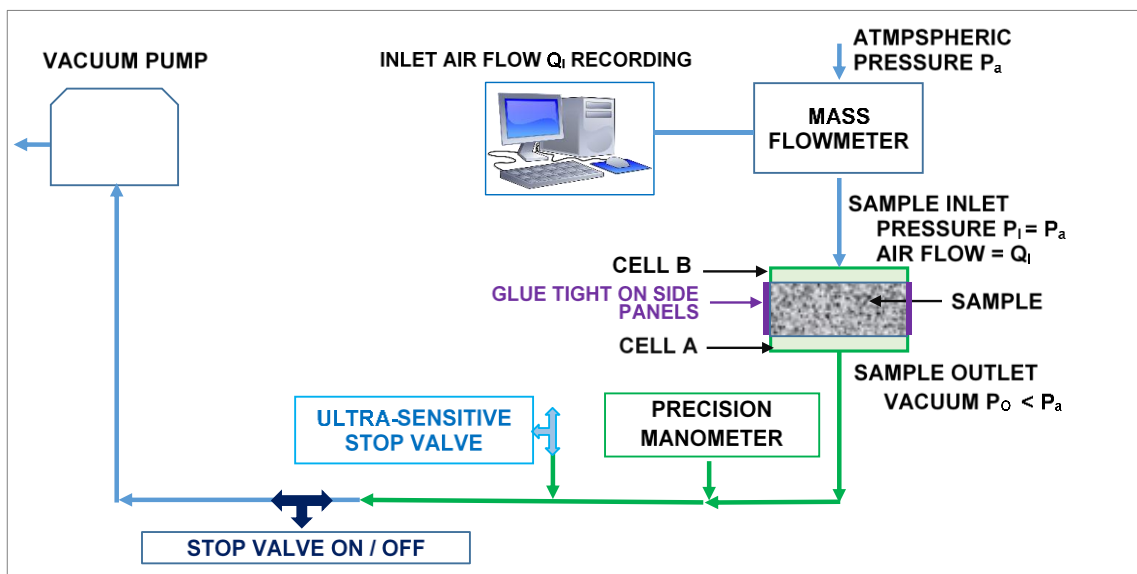


Figure 3: Double cell device for air flow measurement under vacuum

141 The air volume flow measurement protocol is the same as that of the Cembureau  
 142 permeameter. However, the double cell device differs from the Cembureau by the following  
 143 points:

- 144 - The permeability cell is replaced by two cells, one glued to each side face of the sample.
- 145 The lateral faces of the sample are then sealed by means of a fixing / sealing glue. It is
- 146 also possible to use the Cembureau cell when there is no necessity to access the sample
- 147 during the test; this was done in the present study to perform under vacuum

148 measurements in the same conditions as the measurements with the Cembureau  
149 technique on the same sample.

150 - The air supply bottle is replaced by a 4-head diaphragm vacuum pump (pump speed of  
151 13 l/min), which facilitates the mobility of the double cell experimental device  
152 compared to the Cembureau device. The vacuum limit of the pump is 0.5 mbar.

153 The pressure regulator is replaced by an ultra-sensitive needle valve (Series 1300 straight-  
154 through, orifice 1.19 mm in 316 stainless steel). A manometer (Vacuubrand DCP 3000;  
155 pressure range 0.1 to 1080 mbar with digital display from 0.1 to 1100 mbar absolute) is used  
156 to measure the sample outlet pressure. Its accuracy is  $\pm 1$  mbar, which, according to our  
157 results, is sufficient since a variation of 1 mbar induces a maximum variation of 0.1% on the  
158 apparent permeability.

159 The reproducibility of test has been studied [9]. In all cases (plain concrete samples or  
160 reinforced concrete samples), the maximum relative errors obtained are lower than 1.5% for  
161 the air flow  $Q$ , 1.5% for the apparent permeability, and 3% for the TRSS.

### 162 **3.3 Conditioning of samples**

163 To obtain different values of porosity accessible to gas, the samples were tested at different  
164 saturation degrees. To achieve each saturation degree, the samples underwent precise  
165 conditioning [9]. This conditioning was inspired by the literature [25]–[27] trying to reduce  
166 the water gradient and associated cracking during conditioning.

167 The specimens were weighed before and after the permeability measurements. No mass  
168 variations were noted whatever the saturation degree, meaning that the global degree of  
169 saturation stayed constant during the test.

170

## 171 4 Theoretical approach

### 172 4.1 Permeability

#### 173 4.1.1 Principle

174 The coefficient of permeability is defined by Darcy's law. The gas apparent permeability of a  
175 porous medium is calculated using the Hagen-Poiseuille relationship for laminar flow of a  
176 compressible fluid through a porous medium under steady-state conditions [24].

$$k_a = \frac{2 \mu L}{S(P_I^2 - P_O^2)} PQ \quad (\text{Eq. 3})$$

177 where  $PQ$  is the inlet or outlet gaseous flow ( $P_I Q_I$  or  $P_O Q_O$ ),  $P_I$  and  $P_O$  are respectively the  
178 inlet and the outlet pressures ( $\text{N.m}^{-2}$ ),  $Q_I$  and  $Q_O$  are respectively the inlet and the outlet  
179 volume flow rate ( $\text{m}^3.\text{s}^{-1}$ ),  $S$  is the cross-sectional area of the specimen ( $\text{m}^2$ ),  $L$  is the thickness  
180 of the sample in the direction of flow (m), and  $\mu$  is the dynamic viscosity of the fluid ( $\text{N.s.m}^{-2}$ ).  
181

182 The principle of measuring permeability in the steady state is thus based on the measurement  
183 of the air flow  $Q$  crossing a sample subjected to a pressure gradient. The difference between  
184 the two techniques used in this paper lies in the range of pressure applied to create the  
185 gradient and the position where the air flow is measured:

- 186 - Cembureau technique (under pressure): *the absolute applied pressure is the inlet*  
187 *pressure ( $P_I$ )*, which is greater than atmospheric pressure ( $P_a$ ), and the outlet pressure  
188 ( $P_O$ ) is the atmospheric pressure,  $P_a$ . The air flow measured is the outlet one and, in  
189 Figure 2,  $PQ = P_a Q_O$ .
- 190 - Double-cell technique (in vacuum): the absolute inlet pressure ( $P_I$ ) is equal to  
191 atmospheric pressure, *the absolute applied pressure is the outlet pressure ( $P_O$ )*, which is  
192 less than atmospheric pressure (vacuum). The air flow measured is the inlet one and, in  
193 Figure 3,  $PQ = P_a Q_I$  [9].

194 Klinkenberg linear theory (Eq. 4) is then used to determine the intrinsic permeability from the  
195 mean pressure. Klinkenberg established that a linear relationship can be assumed between the  
196 measured gas permeability ( $k_a$ ) and the inverse of the mean pressure ( $1/P_m$ ):

$$k_a = F_{Kl} k_i = k_i \left( 1 + \frac{b_k}{P_m} \right) = \underbrace{k_i}_{\text{Laminar}} + \underbrace{\frac{k_i b_k}{P_m}}_{\text{non-laminar}} \quad (\text{Eq. 4})$$

197 where  $k_a$  is the apparent permeability (also designated  $k_{aP}$  in this paper to mention the  
198 pressure,  $P$ , applied during the test),  $k_i$  is the intrinsic permeability,  $F_{Kl} = 1 + b_k/P_m$  is the

199 Klinkenberg correction factor,  $P_m$  is the mean pressure, and  $b_K$  is the Klinkenberg gas  
 200 slippage factor defined by [28]:

$$b_k = \frac{4c\lambda P_m}{r} = \frac{0.268}{r} \quad (\text{Eq. 5})$$

201 where  $c \approx 1$  [13] and  $\lambda P_m = 0.067 \mu\text{m}\cdot\text{bar}$  for air at a given pressure and  $r$  is the characteristic  
 202 radius in  $\mu\text{m}$ .

#### 203 4.1.2 Mean pressure during measurement

204 The evolution of the apparent permeability with pressure is thus generally plotted as a  
 205 function of the inverse of the mean pressure. As a linear profile of pressure is often assumed  
 206 in steady state, the mean pressure is evaluated by  $(P_I + P_O)/2$ . But, the pressure profile  $P(x)$   
 207 in concrete in the steady state is not linear because of the gas compressibility [16], [29], [30]  
 208 and the mean pressure  $P_m$  should not be taken equal to  $(P_I + P_O)/2$ .

209 In the steady state, the pressure profile  $P(x)$  can be evaluated from the following differential  
 210 equation [16], [31]:

$$\left(\frac{dP}{dx}\right)^2 + P \frac{d^2P}{dx^2} = 0 \quad (\text{Eq. 6})$$

211 One solution of this equation has been derived by Verdier [19] as presented below:

$$P(x) = \left(\frac{P_O^2 - P_I^2}{L}x + P_I^2\right)^{1/2} \quad (\text{Eq. 7})$$

212 where  $P_I$  is the sample inlet pressure and  $P_O$  its outlet pressure.

213 By using the theorem of the mean value, we can deduce the true mean pressure in the steady  
 214 state as follows [9]:

$$P_m = \frac{1}{L} \int_0^L \left(\frac{P_O^2 - P_I^2}{L}x + P_I^2\right)^{1/2} dx \quad (\text{Eq. 8})$$

215 The mean pressure  $P_m$  can thus be evaluated from:

$$P_m = \frac{2}{3} \left(\frac{P_O^3 - P_I^3}{P_O^2 - P_I^2}\right) \quad (\text{Eq. 9})$$

216 This value is used in the following analysis.

217 4.1.3 Flow regime during measurement

218 To evaluate permeability reliably with Klinkenberg theory, the flow regime existing during  
 219 the measurement must be known. The Knudsen number is a dimensionless parameter  
 220 commonly used to classify flow regimes in small pores, where deviation from continuum flow  
 221 is important. This is the case for cement-based materials. It is defined as the ratio of the  
 222 molecular mean free path,  $\lambda$  ( $\mu\text{m}$ ), to a characteristic length, such as pore radius,  $r$  ( $\mu\text{m}$ ), and  
 223 is given by:

$$Kn = \frac{\lambda}{r} = \frac{1}{r} \left( \frac{0.067}{P_m} \right) \quad (\text{Eq. 10})$$

224 Where  $P_m$  is the mean pressure in bar and the mean free path is evaluated by  $\lambda P_m = 0.067$   
 225  $\mu\text{m}\cdot\text{bar}$  for air at a given pressure [28]. The determination of the radius  $r$ , characteristic of the  
 226 percolation in a porous medium such as concrete is often difficult and constitutes a challenge  
 227 [14]. Theoretical and empirical equations can be proposed to approximate this characteristic  
 228 mean radius from a single apparent permeability [9]. The Knudsen number could then be  
 229 calculated based on this equivalent radius and thus on the type of flow regime identified.

230 Flow regimes can be classified according to the Knudsen number as shown in Figure 4.

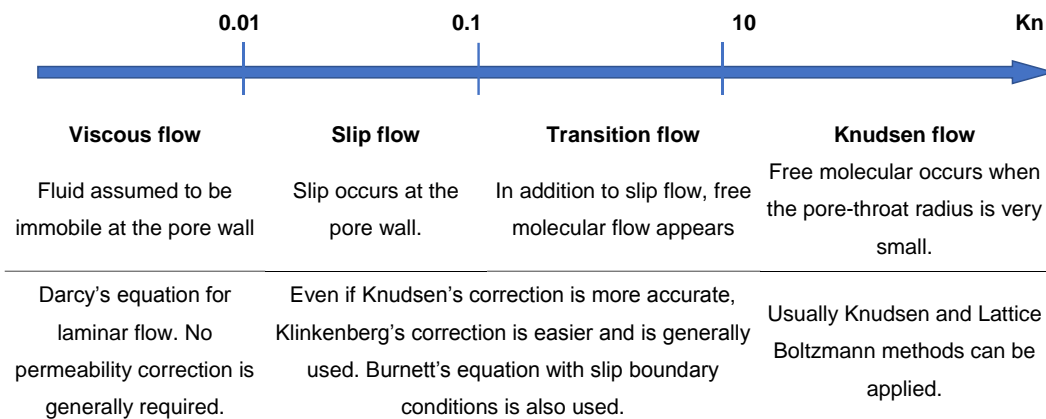


Figure 4: Knudsen number, flow regime classifications for porous media [14], [32], [33]

231 The flow regime in a cementitious porous material is generally a transition flow between  
 232 laminar, slip and molecular regimes [14]. So, in this study, from Figure 4, we firstly make the  
 233 assumption that the Knudsen number lies between 0.1 and 10. This allows us to use the  
 234 Klinkenberg theory for the determination of the intrinsic permeability as is usually done in the  
 235 literature.

236 The range of characteristic radius,  $r$ , that satisfies this condition can be theoretically deduced  
 237 from the Knudsen number range (Eq. 10). By combining the two ranges of pore radius  
 238 calculated (considering the lowest mean pressure used in this paper is 0.67 bar for the  
 239 measurement in vacuum and 1.5 bars for the measurement under pressure), it is theoretically  
 240 assumed here that Klinkenberg's correction can be applied for  $r$  lying between 0.01 and 0.4  
 241  $\mu\text{m}$ . These assumptions on Knudsen number and on the pore radius,  $r$ , have been verified  
 242 from the permeability calculations.  $\text{Kn}$  is always found to be lower than 10 under pressure and  
 243 in a vacuum. The flow regime is then a transition between laminar and molecular flow. It  
 244 indicates that the application of Klinkenberg's theory is possible [9].

#### 245 4.1.4 Comparison of permeability obtained under pressure and under vacuum

246 Relations between Klinkenberg equations (Eq. 4) and (Eq. 5) can be used to establish a  
 247 relation between the reference permeability,  $k_{a2bars}$ , obtained under pressure and the apparent  
 248 permeability obtained in a vacuum,  $k_{aP}$ . As  $4c\lambda P_m = 0.268 \mu\text{m}\cdot\text{bar}$  for any air pressure  
 249 [34], the Klinkenberg equation can be rewritten as:

$$k_a = k_i \left( 1 + b_k \frac{1}{P_m} \right) = k_i \left( 1 + \frac{4c\lambda P_m}{r} \frac{1}{P_m} \right) = k_i \left( 1 + \frac{0.268}{r} \frac{1}{P_m} \right) \quad (\text{Eq. 11})$$

250 So, the ratio between the apparent permeability for  $P_1 = 2$  bars and the apparent permeability  
 251 for a given  $P_1 = P$  is:

$$\frac{k_{a2bars}}{k_{aP}} = \frac{k_i \left( 1 + \frac{0.268}{r} \frac{1}{1.568} \right)}{k_i \left( 1 + \frac{0.268}{r} \frac{1}{P_m} \right)} = C_P \quad (\text{Eq. 12})$$

252 This ratio between apparent permeability is then:

$$k_{a2bars} = C_P k_{aP} \quad (\text{Eq. 13})$$

253 where  $C_P$  is a theoretical, non-dimensional coefficient:

$$C_P = \frac{r + 0.171}{r + 0.268/P_m} \quad (\text{Eq. 14})$$

254 where  $r$  is the characteristic radius and  $P_m$  is the mean pressure in bar.

255 Figure 5 presents the evolution of  $C_P$  with the characteristic radius,  $r$ .

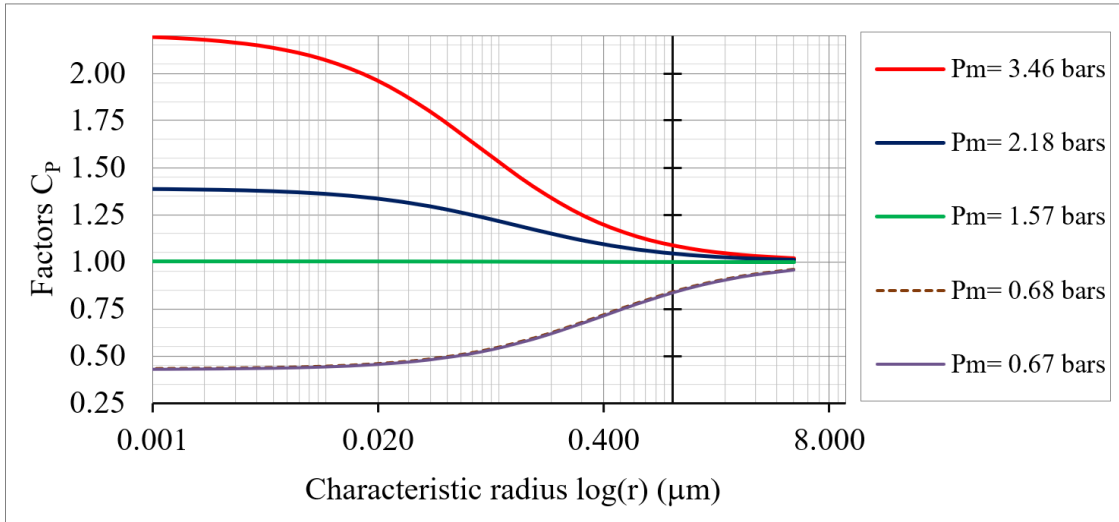


Figure 5: Evolution of  $C_P$  as function of characteristic radius  $r$

256 When  $r$  is very small,  $C_P$  is high for under pressure measurement: the slip flow evaluated  
 257 through the Klinkenberg slippage factor,  $b_K$ , is high. This is in accordance with the evolution  
 258 of the Knudsen number:  $Kn$  is inversely proportional to radius  $r$  (Eq. 10), so  $Kn$  is higher for  
 259 smaller  $r$ . When  $r$  increases, the Knudsen number decreases, the slippage factor  $b_K$  also  
 260 decreases, and the flow regime tends to laminar flow. For very large radius, the apparent  
 261 permeability is equal to the intrinsic permeability. This occurs with highly porous media, such  
 262 as rubberized cement-based composite [35].

263 In the range assumed in this paper for the pore radius  $r$ , in cementitious materials ( $r$  lies  
 264 between 0.01 and 0.4  $\mu\text{m}$  - this assumption has been verified in [9]) the coefficient  $C_P$  shows  
 265 small variations (Figure 5). A mean value of  $C_P$  can be used, evaluated with the mean value  
 266 theorem as:

$$\text{Mean value of } C_P = \frac{1}{0.4 - 0.01} \int_{0.01}^{0.4} \left( \frac{r + 0.171}{r + 0.268/P_m} \right) dr \quad (\text{Eq. 15})$$

267 The mean values of  $C_P$  are presented in Table 1. Without knowing the real value of  $r$ , the  
 268 relation of (Eq. 13) can be used to evaluate the apparent permeability as a function of the  
 269 mean pressure given in Table 1.

270

271 **Table 1.** Main values of  $C_P$  when  $r$  is between 0.01 and 0.4  $\mu\text{m}$  as a function of the mean  
 272 pressure  $P_m$

Measurement technique	Absolute Pressure (bars)				$C_P$ (Eq. 15)
	Inlet $P_I$	Outlet $P_O$	Mean $P_m$ $(P_I + P_O)/2$	Mean $P_m$ (Eq. 9)	
Cembureau	2.0		1.51	1.57	1.00
	3.0	1.013	2.01	2.18	1.17
	4.0	(1 atm)	2.51	2.81	1.30
	5.0		3.01	3.46	1.41
Double cell		0.0005	0.51	0.67	0.61
	1.013	0.050	0.53	0.68	0.61
	(1 atm)	0.150	0.58	0.69	0.62
		0.250	0.63	0.71	0.63

273

274 4.1.5 Permeability determination

275 We can thus propose the calculation of intrinsic permeability from a single reference value  
 276  $k_{a2bars}$ . Using (Eq. 13) and  $C_P$  values in Table 1,  $k_{a2bars}$  can be calculated from any apparent  
 277 permeability obtained under vacuum with the double cell technique. With (Eq. 13) and  $C_P$   
 278 values in Table 1, the apparent permeabilities  $k_{a3bars}$ ,  $k_{a4bars}$ ,  $k_{a5bars}$  can be calculated from a  
 279 single  $k_{a2bars}$ . The intrinsic permeability  $k_i$  can then be extrapolated to infinite pressure by  
 280 plotting  $k_{a2bars}$ ,  $k_{a3bars}$ ,  $k_{a4bars}$ ,  $k_{a5bars}$  as a function of the inverse of the mean pressure  
 281 (Klinkenberg theory). In the following, the calculated coefficients  $C_P$  are validated on the  
 282 experimental database established in this paper and then on some literature data.

283 **4.2 Measurement of porosity accessible to gas**

284 Porosity accessible to gas can be calculated from the TRSS and apparent permeability. This  
 285 equation is based on the balance of the number of air particles flowing in the porous network  
 286 due to the application of the pressure gradient to the steady state. For the sake of simplicity,  
 287 only the demonstration based on measurement with the double-cell technique under vacuum  
 288 is presented. The same demonstration can be made under pressure and gives the same results  
 289 as the solution does not imply any particular assumptions.

290 The initial conditions for the test with the double-cell technique are first recalled:

- 291 - The flow is unidirectional along the length,  $L$ , of the sample.

- 292 - The pressure profile in the concrete is  $P(x)$ . The boundary conditions are those
- 293 described in Figure 3: the inlet pressure,  $P_I$ , is equal to the atmospheric pressure,  $P_a$ , at
- 294  $x = 0$  and the outlet pressure is  $P_O$  at  $x = L$ .
- 295 -  $t$  is the time during which the vacuum is applied; its maximum value is the TRSS
- 296 (noted  $t_{RSS}$  in the following equations). It is the time beyond which the mass flow is
- 297 constant in any cross section of the sample. It is also the time beyond which the
- 298 pressure profile in the concrete no longer varies.
- 299 -  $Y$  is the thickness of the sample reached by the vacuum pressure at any time  $t$ .

300 Figure 6 shows the evolution of pressure profile in concrete during air flow measurement.

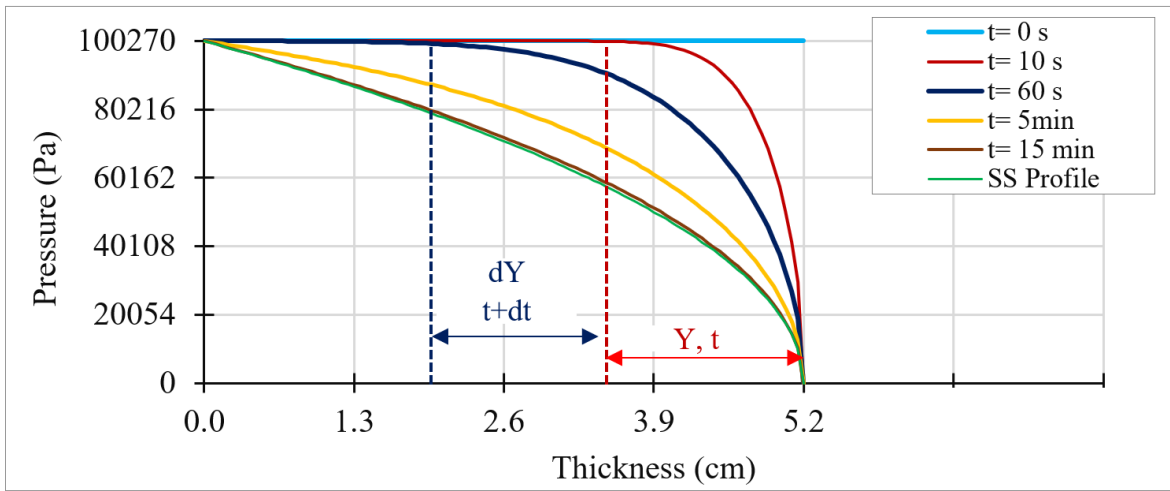


Figure 6: Evolution of pressure profiles until steady state for a sample ( $L = 5.2$  cm) [9]

301 At the beginning of vacuum application,  $t = 0$  s and the depth impacted by the vacuum is  $Y_0 =$

302 0. At any moment  $t$  ( $t > 0$ ) at the beginning of the application of the vacuum (10 s for

303 example), a depth  $Y$  is impacted by the vacuum.

304 The air volume of the pores impacted during this time  $t$  and the corresponding number of air

305 particles are, respectively:

$$V = AY\phi_g \quad (\text{Eq. 16})$$

$$N = \frac{P_m \cdot V}{B \cdot T} = \frac{P_m}{BT} SY\phi_g \quad (\text{Eq. 17})$$

306 where  $P_m$  is the mean pressure at depth  $Y$  impacted by the vacuum during  $t$  (s),  $V$  is the air

307 volume in pores of the zone impacted by the vacuum ( $\text{m}^3$ ),  $S$  is the area of the sample section,

308  $\phi_g$  is the porosity accessible to gas and  $B$  is the Boltzmann number.

309 During any time interval  $dt$ , the vacuum affects a new front of air particles  $dN$  since the depth

310  $Y$  increases by  $dY$ . From (Eq. 17), it can be written:

$$dN = \frac{S \phi_g}{BT} P_m dY \quad (\text{Eq. 18})$$

311 Also, the Hagen-Poiseuille equation (Eq. 3) gives the volume,  $dV$ , of gas flowing in the cell  
312 under the pressure gradient  $(P_1 - P_2)$  over the distance  $Y$  into concrete.

$$dV = \frac{k_{ad} S}{2\mu} \frac{P_1^2 - P_0^2}{P_0 Y} dt \quad (\text{Eq. 19})$$

313 This volume of air is at the outlet pressure  $P_0$  and, in terms of the number of air particles, it  
314 corresponds to:

$$dN = \frac{P_0 dV}{BT} \quad (\text{Eq. 20})$$

315 From the three previous relationships, it can be written:

316

$$dN = \frac{P_0 dV}{BT} = \frac{P_0 k_{ad}}{BT 2\mu} \frac{P_1^2 - P_0^2}{P_0 Y} S dt = \frac{S \phi_g}{BT} P_m dY \quad (\text{Eq. 21})$$

317 After simplification, it can be deduced that:

$$Y dY = \frac{k_a (P_1^2 - P_0^2)}{2\mu \phi_g P_m} dt \quad (\text{Eq. 22})$$

318 In the steady state, the mean pressure  $P_m$  has reached its stabilized value so, by integrating the  
319 previous relation, the depth affected by the vacuum at any time  $t$  can be calculated from:

$$\frac{1}{2} Y^2 = \frac{k_a (P_1^2 - P_0^2)}{2\mu \phi_g P_m} t \quad (\text{Eq. 23})$$

320 At the steady state,  $t = t_{RSS}$ ,  $Y = L$ , and  $P_m$  is given by (Eq. 9), so the porosity can be evaluated  
321 from:

$$\phi_g = \frac{k_a (P_1^2 - P_0^2)}{\mu L^2 P_m} t_{RSS} = \frac{3 k_a (P_1^2 - P_0^2)^2}{2 \mu L^2 (P_1^3 - P_0^3)} t_{RSS} \quad (\text{Eq. 24})$$

322 Considering the Hagen-Poiseuille equation (Eq. 3),  $\phi_g$ , the porosity accessible to gas, can also  
323 be written as a function of the measured air flow  $PQ_V$ :

$$\phi_g = \frac{1}{SL} \left( \frac{2PQ}{P_m} t_{RSS} \right) = \frac{3PQ}{SL} \left( \frac{P_0^2 - P_1^2}{P_0^3 - P_1^3} \right) t_{RSS} \quad (\text{Eq. 25})$$

324 where the gaseous flow  $PQ_V$  is the same as used in (Eq. 3). It is equal to  $P_a Q_0$  if the  
325 Cembureau technique is used and  $P_a Q_I$  with the double-cell technique. Regarding the sample,

326  $SL$  is the total apparent volume and the expression  $2PQt_{RSS}/P_m$  can leads then to an  
327 estimation of the volume of percolating pores.

## 328 **5 Results and discussion**

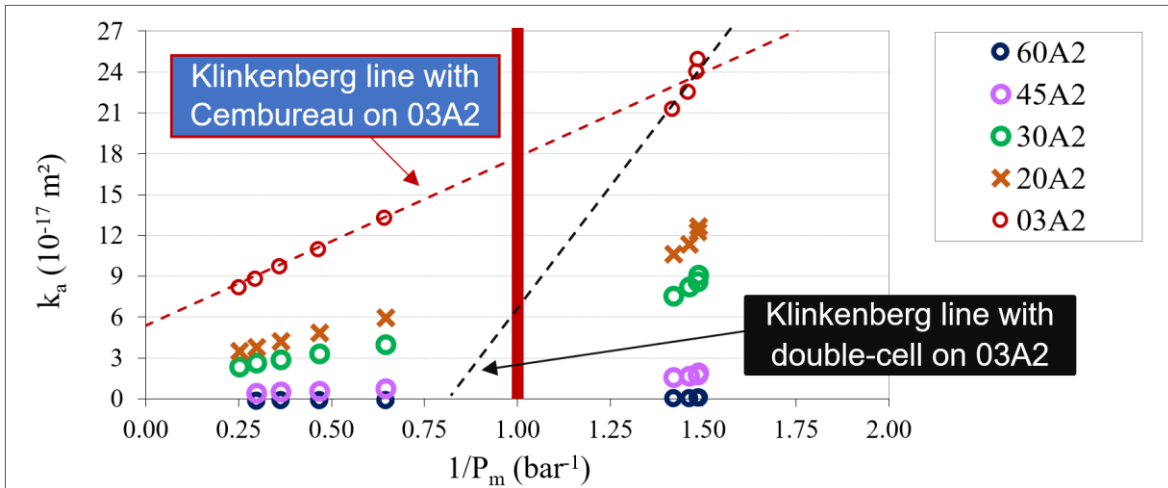
### 329 **5.1 Permeability under vacuum and under pressure**

#### 330 5.1.1 Experimental results

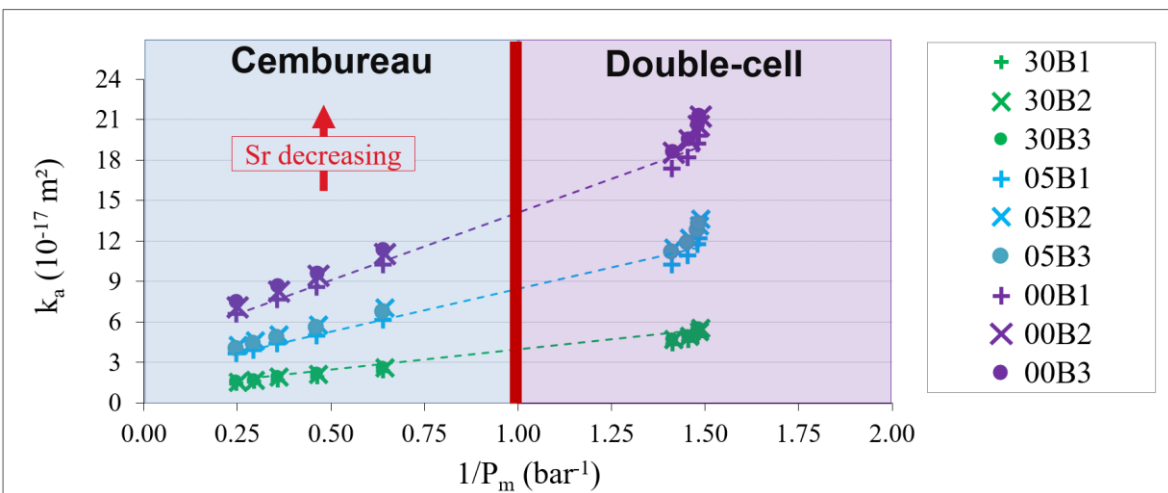
331 Figure 7 presents the apparent permeability,  $k_a$ , as a function of the inverse of the mean  
332 pressure  $P_m$  for one sample of each type: one plain sample from batch A (a), one plain sample  
333 from batch B (b), one each of reinforced samples R2, R3 and R5 (c). The results obtained on  
334 the other samples led to the same analysis.

335 The apparent permeability under vacuum ( $1/P_m > 1$ ) is always greater than the permeability  
336 under pressure obtained under pressure with the Cembureau permeameter ( $1/P_m < 1$ ). This  
337 result is consistent with the evolution of the molecular and slip flows as the non-laminar  
338 contribution to air flow is inversely proportional to the pressure (Eq. 4). As the mean pressure  
339 with the double-cell under vacuum is always lower than the mean pressure in conditions of  
340 under pressure (Table 1), the apparent permeability under vacuum conditions must be greater  
341 than the one obtained under pressure.

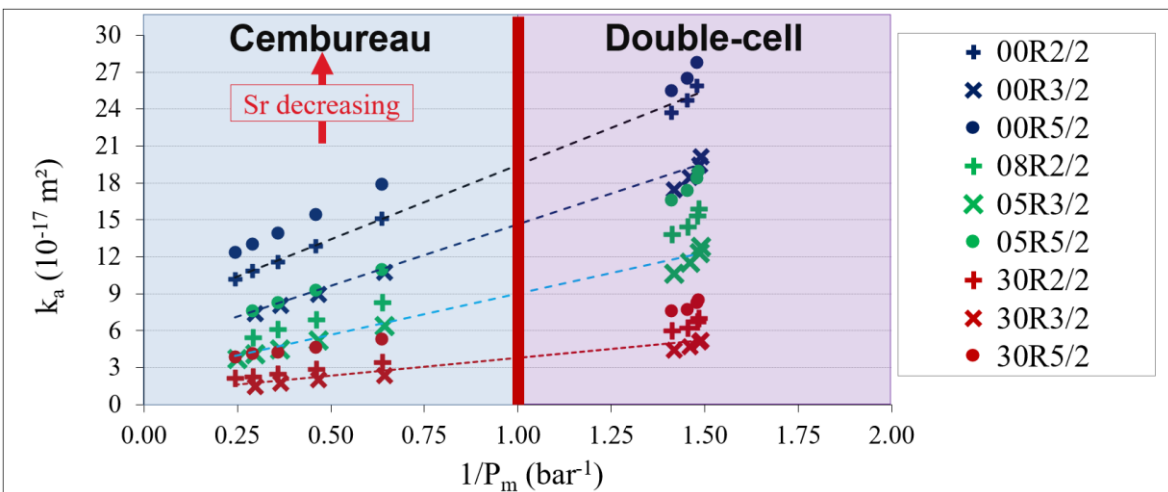
342



(a)



(b)



(c)

Figure 7: Apparent permeability and Klinkenberg lines for plain samples of two different batches (a and b) and for samples with embedded steel bars (c)

343 As illustrated in Figure 7-a, if Klinkenberg lines are plotted from the apparent permeability  
344 obtained under vacuum, high slopes are obtained, and a loss of linearity is observed: the non-  
345 laminar contribution is greater in a vacuum, and molecular flow increases as the vacuum  
346 becomes harder. This mechanism leads to obtain higher slopes under vacuum than under  
347 pressure. As a result, linear extrapolation of the experimental points leads to negative intrinsic  
348 permeability. This representation of Klinkenberg theory does not allow intrinsic permeability  
349 to be estimated but seems indicative of the evolution in molecular flow with the vacuum.  
350 Moreover, it highlights the difference of flow nature between the two techniques.

351 Nevertheless, for each sample at any saturation degree, the apparent permeability under  
352 vacuum obtained with the double-cell technique and plotted versus the inverse of the mean  
353 pressure is located near the reference Klinkenberg line established from the Cembureau  
354 measurement. For low pressures, the points deviate from the line, which also reflects the  
355 limits of Klinkenberg's approach at these pressures.

356 Experimental results can also be analysed with regard to the relative permeability for the  
357 quantification of the permeability evolution with saturation degree. It is defined as:

$$k_{Sr,Rel} = \frac{k_{Sr}}{k_{Srf}} \quad (\text{Eq. 26})$$

358 where  $k_{Sr,Rel}$  is the relative permeability as a function of the saturation degree,  $k_{Sr}$  is the  
359 permeability at a given saturation degree and  $k_{Srf}$  is the permeability at the lowest saturation  
360 degree reached during the drying. The  $k_{Srf}$  considered in this study is obtained for  $Sr = 3\%$   
361 after drying at 80 °C to constant mass.

362 As it has been well described in the literature [2], [9], [19], [36], the concrete permeability  
363 increases when the saturation degree decreases: during drying, the flow paths are released  
364 from the free water and the air flow through concrete can increase. Moreover, drying can  
365 induce damage and micro-cracking that increases the percolating network. This expected  
366 result is effectively obtained for the two techniques. Figure 8 presents the relative apparent  
367 permeability for the two techniques used in this paper for  $P_l = 2$  bars (Cembureau) and  $P_o =$   
368 250 mbars (double-cell) and the relative intrinsic permeability.

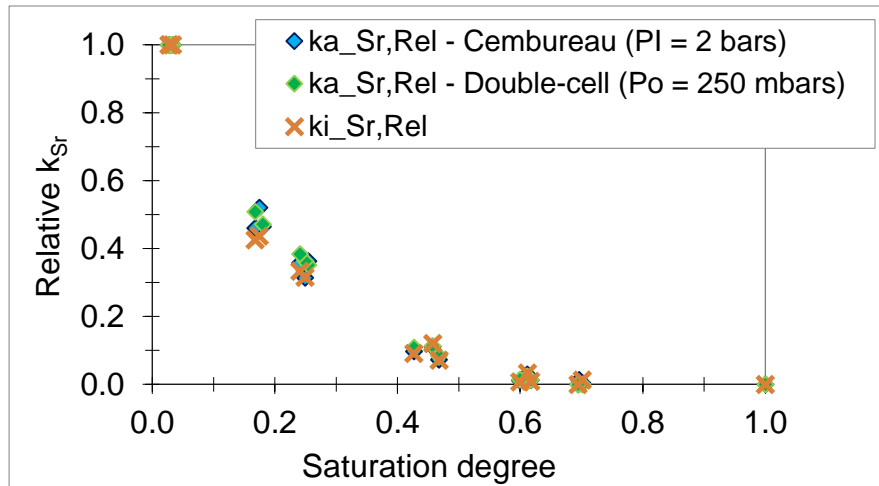


Figure 8: Relative permeability according to saturation degree

369 Whatever the type of permeability used (intrinsic permeability according to Klinkenberg,  $k_i$ ,  
 370 apparent permeability,  $k_{a2bars}$ , with the Cembureau technique, apparent permeability,  $k_{a250mbars}$ ,  
 371 with the double-cell technique), the evolutions of the relative permeability with the saturation  
 372 degree were similar. This means that, without any other numerical processing, the apparent  
 373 permeability obtained with the double-cell technique (or with the Cembureau technique) can  
 374 be used to characterize the relative permeability.

### 375 5.1.2 Validation of the theoretical approach for permeability

376 The objective is to determine  $k_{a2bars}$  and  $k_i$  from any single apparent permeability given by the  
 377 double-cell technique. Here is an example of the calculation protocol when the input data is  
 378 apparent permeability obtained with the double cell for  $P_O = 250$  mbars:  $k_{a250mbars}$ .

- 379 - For  $P_O = 250$  mbars,  $C_P = 0.63$  in Table 1. Then (Eq. 13) gives the value of  $k_{a2bars}$ .
- 380 - With this value of  $k_{a2bars}$  and with (Eq. 13), we calculate:  $k_{a3bars}$  ( $C_P = 1.17$  in Table 1),  
 381  $k_{a4bars}$  ( $C_P = 1.30$  in Table 1),  $k_{a5bars}$  ( $C_P = 1.41$  in Table 1)

382 Figure 9 presents the results of  $k_{a2bars}$  and  $k_i$  predictions when the input data are  $k_{a250mbars}$  or  
 383  $k_{a150mbars}$  or  $k_{a0.5mbar}$ .

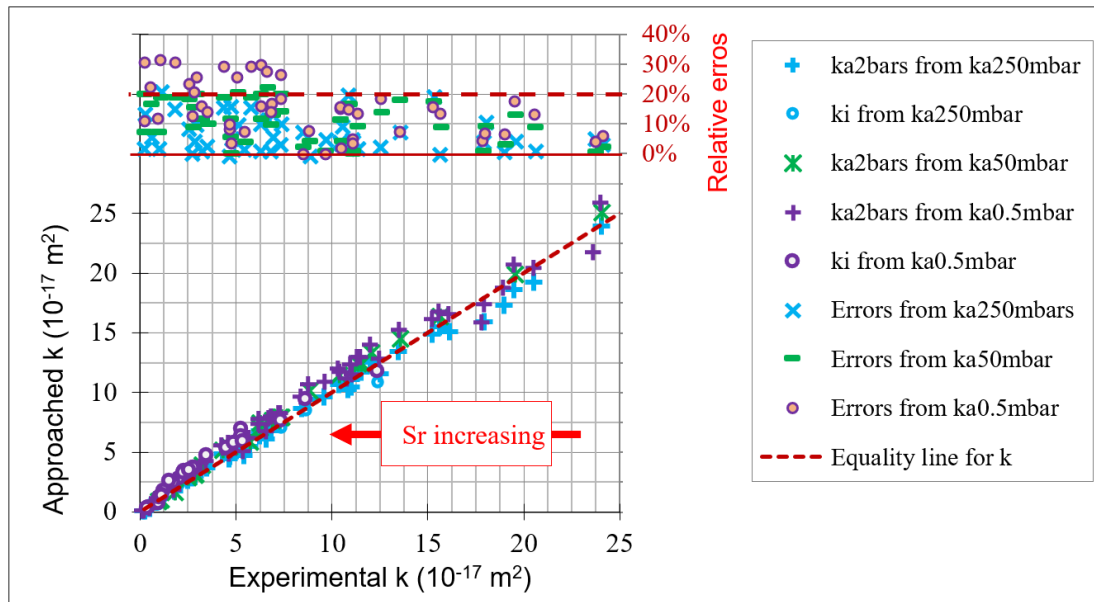


Figure 9. Comparison of experimental and approached permeability

384 The relative error between the permeability approximated with the proposed method and the  
 385 experimental value  $k_{a2bars}$  is also presented in Figure 9:

- 386 - The lowest vacuum pressure leads to the greatest relative error: this is in accordance  
 387 with the assumption on flow regime. If the vacuum pressure is reduced, the flow rate  
 388 no longer increases (between  $P_O = 50$  mbar and  $P_O = 0.5$  mbar the permeability  
 389 increases by only 3%) whereas the molecular flow becomes more and more important,  
 390 leading to the limits of use of Klinkenberg's theory. Then, for  $k_{a2bars}$  and  $k_i$  prediction  
 391 with the double-cell technique, measurement should be performed with  $P_O$  equal to or  
 392 greater than 50 mbars.
- 393 - Using permeability for  $P_O$  equal to or greater than 50 mbars, the relative error is  
 394 always lower than 20%. Its mean value is about 7% and 12% when the calculations  
 395 are done with  $k_{a250bars}$  and  $k_{a50mbar}$ , respectively, which is considered as acceptable in  
 396 this paper because of the usual deviation obtained on permeability measurement,  
 397 which can reach 20% on 3 samples of a given batch.

398 The values of the coefficients  $C_P$  (Table 1) are thus validated on the concrete studied in this  
 399 work for various saturation degrees. The proposed approach makes it possible to estimate the  
 400 apparent and intrinsic permeability from one value of apparent permeability.

401 The theoretical approach is also validated on experimental literature values. The objective is  
 402 to determine apparent permeability at any pressure and the intrinsic permeability  $k_i$  from a  
 403 single apparent permeability  $k_{a2bars}$  using (Eq. 13) and the value of  $C_P$  presented in Table 1,

404 for concrete of other experiments drawn from the literature. The apparent permeability must  
 405 be calculated separately for inlet pressures,  $P_i$ , equal to 3, 4 and 5 bars:

- 406 - Calculation of  $k_{a3bars}$ :  $P_m = 2.18$  and  $C_p = 1.18$  in Table 1,
- 407 - Calculation of  $k_{a4bars}$ :  $P_m = 2.81$  and  $C_p = 1.31$  in Table 1,
- 408 - Calculation of  $k_{a5bars}$ :  $P_m = 3.46$  and  $C_p = 1.42$  in Table 1,
- 409 - Plot of calculated apparent permeability versus  $1/P_m$  to deduce  $k_i$ .

410 Figure 10 presents the materials and the results ( $k_{a5bars}$  and  $k_i$ ; the predicted  $k_{a4bars}$  and  $k_{a3bars}$   
 411 show the same concordance) of this calculation protocol.

412 Porosity values are given for information. Porosity shows the porous extent of the concrete  
 413 used to validate the value of  $C_p$  proposed in this work. The relative errors between the  
 414 experimental values and the values evaluated by this method is less than 20%, which is  
 415 acceptable according accuracy on experimental measurement [16].

416

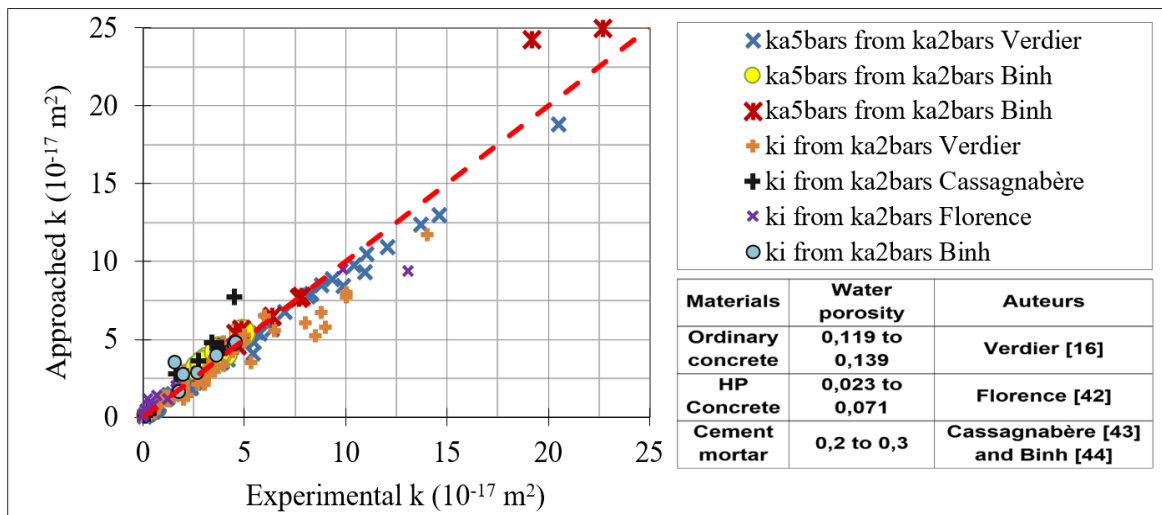


Figure 10: Validation of  $C_p$  values on literature data

417

## 418 5.2 Porosity accessible to gas

### 419 5.2.1 Experimental results of the Time to Reach Steady State (TRSS)

420 The porosity can be evaluated from the Time to Reach Steady State (TRSS) with (Eq. 25).  
 421 First, Figure 11-a compares the Time to Reach Steady State (TRSS) obtained with the two  
 422 techniques studied in this paper (under pressure in abscissa and under vacuum in ordinate).  
 423 The TRSS obtained with the two techniques are almost equal but the TRSS with Cembureau  
 424 are always slightly higher than those obtained with the double-cell technique. The apparent

425 permeability under vacuum (obtained with double-cell) is always higher than the permeability  
 426 obtained under pressure (with Cembureau). As the porous network is the same, the time  
 427 necessary for the gas particles to cross the network (TRSS) is shorter under vacuum. As for  
 428 permeability, it is interesting to analyse the relative TRSS. In this work, the relative TRSS  
 429 was defined as the relative permeability (ratio of the TRSS obtained for a given saturation  
 430 degree to the TRSS obtained for sample with a saturation degree of 3%).

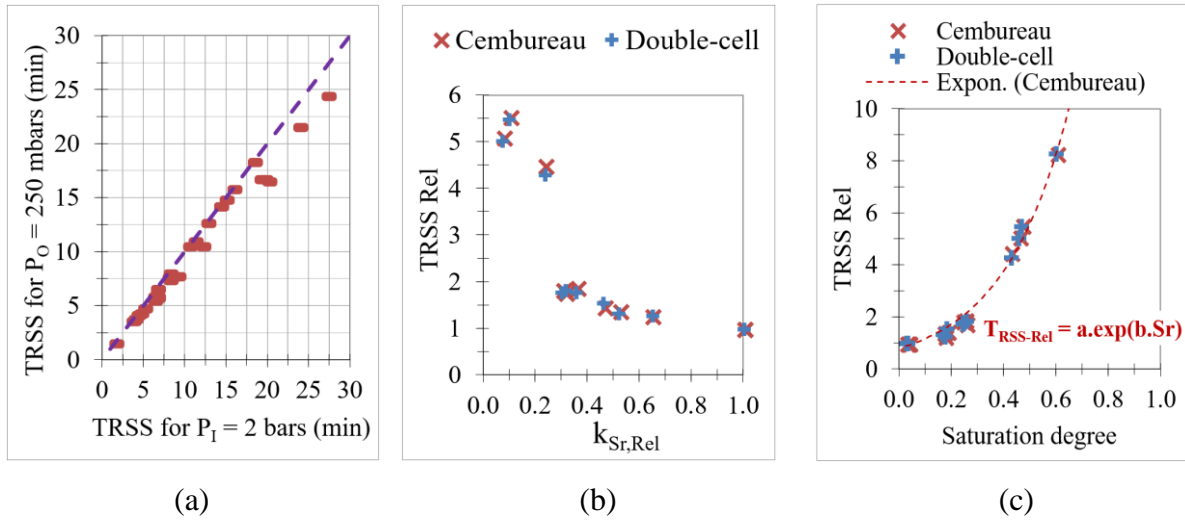


Figure 11: TRSS with double-cell and Cembureau techniques (a), permeability (b) and TRSS as function of saturation degree (c)

431 Figure 11-b presents the evolution of relative TRSS as a function of the relative permeability.  
 432 When the relative permeability increases, the TRSS decreases. Considering that the TRSS is a  
 433 function of the percolation path (tortuosity, constrictivity, rugosity, pore distribution), the  
 434 impact of the pore tortuosity appears to be reduced for the highest permeability. The steady  
 435 state is reached quickly when the air molecules encounter few obstacles in the porous  
 436 network. Figure 11-c presents the evolution of TRSS as a function of the saturation degree  
 437 and confirms this analysis. When the saturation degree decreases, the flow paths become  
 438 progressively free of water and so air molecules encounter fewer obstacles and the steady  
 439 state is reached faster, and permeability increases.

440 An empirical model of relative TRSS can be proposed:

$$T_{RSS_{Rel}} = a \cdot \exp(b \cdot Sr) \quad (\text{Eq. 27})$$

441 where  $a$  and  $b$  are two parameters established experimentally for each type of material. For  
 442 the two batches of concrete tested in this paper  $a$  and  $b$  values are 0.78 and 3.92 for the plain  
 443 samples (Figure 11-c). It is important to note that the same values of  $a$  and  $b$  are obtained  
 444 with the Cembureau technique as with the double-cell technique. The double-cell technique

445 can characterize the evolution of the transport properties of concrete according to saturation  
 446 degree.

447 5.2.2 Validation of the theoretical approach for porosity

448 Figure 12 presents the porosity accessible to gas evaluated from TRSS (Eq. 25) for plain  
 449 samples with the two techniques (Cembureau and double-cell) and the theoretical porosity  
 450 evaluated from the total porosity accessible to water ((Eq. 1) and (Eq. 2)). Apparent  
 451 permeability  $k_{a2bars}$  is also plotted in blue on a secondary axis, for comparative analysis in  
 452 Figure 12. In the case of very low permeability, the measurement of air flow may be not  
 453 possible (case of sample 60B1 with the double-cell technique in Figure 12). The air flow is  
 454 then equal to zero and there is no evaluation of TRSS, so the porosity deduced from the new  
 455 approach is equal to zero, which is not necessarily true.

456 When the measurement of air flow is possible with the two techniques, the porosity accessible  
 457 to gas obtained with both techniques is very similar (Figure 12): the absolute dispersion  
 458 between the two techniques is  $0.4\% \pm 0.2\%$ . This is within the range of the accuracy on the  
 459 measurement of porosity accessible to gas with the TRSS as presented in Figure 12.  
 460 Concerning the comparison with the measurement under water, the results show similar trends  
 461 according to the sample.

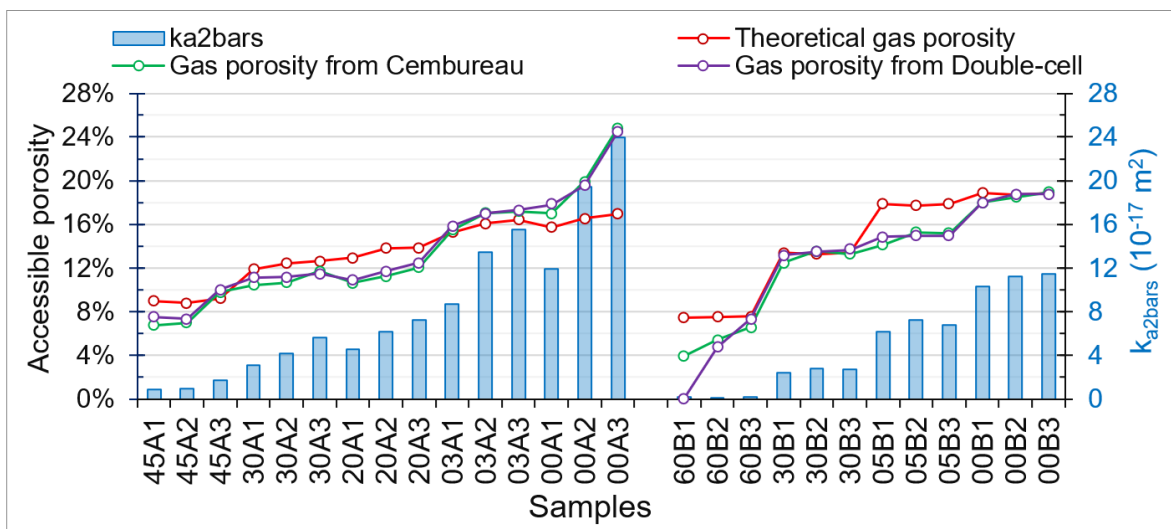


Figure 12: Accessible porosity from different models on plain samples for two batches A and B (theoretical porosity is evaluated from total porosity accessible to water (Eq. 1))

462 For most of the samples, the porosity deduced from measurement under water is higher than  
 463 the porosity measured by gas transfer (Figure 12). This can be explained by the fact that the  
 464 water porosity is the total accessible porosity whereas the porosity accessible to gas is the  
 465 porosity that contributes to percolation paths during permeability test.

466 During the usual measurement, water can partly fill some dead arms. For the porosity  
467 calculated from TRSS through a permeability test, the porosity evaluated has to contribute to  
468 the gas transfer paths. As a result, theoretical porosity deduced from water porosity evaluates  
469 both open connected porosity and open non-connected porosity, while the porosity deduced  
470 from the TRSS is very little affected by the open non-connected porosity. Thus, the porosity  
471 calculated from the TRSS seems to be more representative of open-connected porosity. This  
472 approach should be validated on other materials such as porous ceramics.

473 In some cases, the porosity deduced from measurement under water is smaller than the  
474 porosity measured by gas transfer. This is mainly the case for saturation degrees lower than  
475 3% for the first batch (A) for samples presenting the largest permeability (Figure 12). It is  
476 particularly marked for two samples. The high permeability measured in these samples can be  
477 explained by the creation of preferential paths of transfer during the last drying periods at 105  
478 °C [40], [41]. Such paths can have large impacts on the transfer, and thus on the porosity  
479 deduced from transfer, while the consequences for the apparent porosity volume are very  
480 slight.

481 A comparison between the data of samples of the two batches 00A and 00B can complete this  
482 analysis. It introduces the problem of the analysis of the permeability from water porosity.  
483 The water porosity of samples 00B (around 19%) is higher than the water porosity of samples  
484 00A (around 16%), but the permeability of samples 00B ( $12 \times 10^{-17} \text{ m}^2$ ) is lower than the  
485 permeability of samples 00A (around  $22 \times 10^{-17} \text{ m}^2$ ). This points out that the water porosity  
486 cannot be effectively representative of gas percolation paths and so of gas permeability.

487 This result is more appreciable when we consider the results obtained on reinforced concrete  
488 samples (Figure 13). Previous analyses have shown that only significant preferential  
489 percolation paths can explain the differences of permeability of these samples [9], [19]. In  
490 Figure 13, samples 30B, 05B and 00B are plain samples while all the other results are  
491 obtained on reinforced samples (Figure 1). It appears clearly that the theoretical porosity  
492 accessible to gas (deducted from the water porosity) cannot explain the changes in  
493 permeability of these reinforced samples. The theoretical porosity indicates that the reinforced  
494 samples and the plain samples have approximately the same porosity while the permeability  
495 of reinforced samples is sometimes twice that of plain samples.

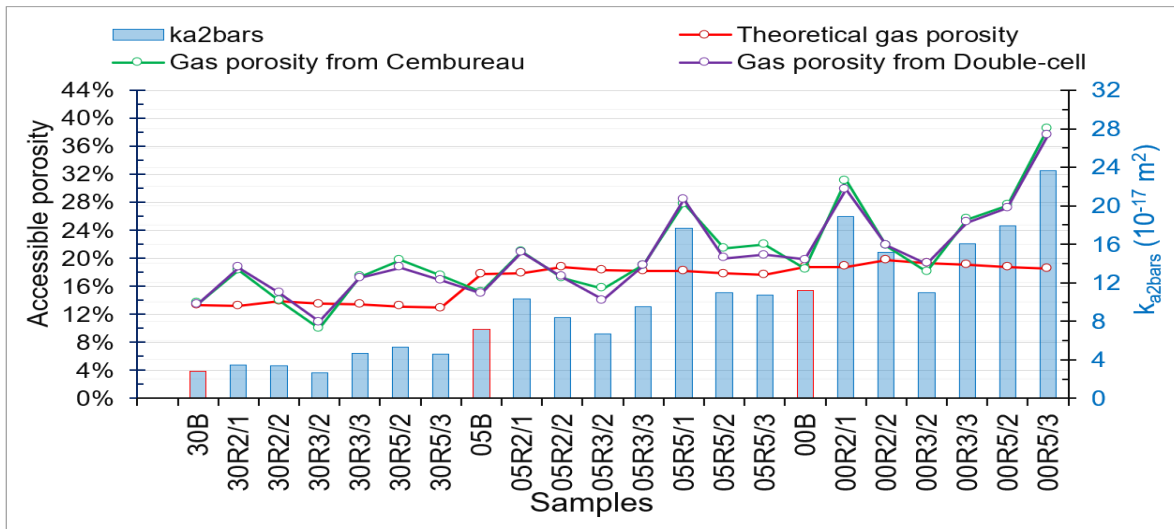


Figure 13: Accessible porosity calculated from water porosity and from TRSS

496 Only the porosities calculated from the TRSS as proposed in this study are sensitive to the  
 497 defect created by steel bar in these samples and enable the samples to be distinguished from  
 498 one another. The porosity calculated from apparent permeability and the TRSS thus appears  
 499 to be more representative of the gas percolation paths.

### 500 5.2.3 Discussion

501 There are some theoretical limits on the proposed approach for porosity calculation. In  
 502 presence of very high permeability or damaged samples, the TRSS should be much reduced  
 503 and so its experimental evaluation could be tainted with error. The lowest value of TRSS in  
 504 this paper was around 250 seconds with a maximum relative error equal to 3%, corresponding  
 505 to an absolute error of 7.5 seconds. For samples with TRSS around 30 seconds [31], and with  
 506 an absolute error of 7 seconds, the relative error becomes about 23%. This may lead to a  
 507 considerable error in the porosity calculation. Another limit of the proposed approach is that  
 508 the porosity calculated from TRSS is the porosity accessible to gas at the moment of the  
 509 permeability test for a given saturation degree.

510 Relative permeability can be assessed as a function of saturation degree [42] (Figure 8). In  
 511 this paper, it has been showed that the relative TRSS can also be evaluated as a function of  
 512 saturation degree (Figure 11-c). Combining these two empirical laws and the theoretical  
 513 relation between permeability, porosity and TRSS (Eq. 24) can lead to consistent prediction of  
 514 the porosity accessible to gas for a concrete. For the purpose of more reliable modelling of  
 515 transport into partially saturated concrete, there are two principal input data [29]: the  
 516 permeability and the porosity. When the given porosity is not representative of the path

517 accessible to gas, a third experimental data can be used to deduce the porosity accessible to  
518 gas transfer (Eq. 24): the time to reach steady state (TRSS).

## 519 **6 Conclusion**

520 The main objectives of this study have been to compare different techniques to determine the  
521 apparent and intrinsic permeability and the porosity of concrete. Three specific points were  
522 studied: establishment of an experimental database on concrete air permeability and time to  
523 reach steady state, analysis of transfer properties through permeability calculations, and  
524 assessment of the porosity accessible to gas.

525 For the first time, air flow through concrete has been measured in vacuum with a double-cell  
526 device and under pressure with the Cembureau technique in the steady state for identical  
527 samples. The apparent permeability in low vacuum at steady state was calculated from the  
528 Hagen Poiseuille equation and compared to the under-pressure technique for the same  
529 samples. This apparent permeability obtained in vacuum from the double-cell was clearly  
530 efficient for the determination of the relative permeability.

531 The second goal of this paper has been the analysis of transfer properties through permeability  
532 calculation. The characteristic apparent permeability,  $k_{a2bars}$ , was calculated from one apparent  
533 permeability given by the double-cell technique. This characteristic permeability was  
534 compared to the apparent permeability measured directly with the Cembureau technique. An  
535 original relation between apparent permeability at different pressures was proposed and  
536 validated, and the results showed good agreement between prediction and experimental  
537 measurements.

538 Concerning the Time to Reach Steady State (TRSS), this study shows that this parameter can  
539 be used to analyse the percolation paths regardless of the techniques used (double-cell or  
540 Cembureau). An empirical relation was established for the relative TRSS as a function of  
541 saturation degree. The porosity accessible to gas was calculated from a new relation between  
542 the TRSS and the apparent permeability (or volumetric air flow). The results obtained from  
543 the Cembureau technique and those obtained with the double-cell technique were in good  
544 concordance. Moreover, these results obtained show that this porosity should be more  
545 convincing than the water porosity for the evaluation of the percolation paths accessible to  
546 gas.

## 547 **7 Acknowledgment**

548 The authors acknowledge the financial support provided by the project “Non-destructive  
549 evaluation of containment of nuclear power plants” (ENDE) financed by the Programme  
550 Investissement d’Avenir (PIA – Centre National de la Recherche Scientifique, délégation  
551 Provence et Corse, France).

## 552 **8 Conflict of Interest statement**

553 **Conflict of Interest:** The authors declare that they have no conflict of interest.

## 554 **9 References**

- 555 [1] H. Hilsdorf and J. Kropp, *Performance Criteria for Concrete Durability*. CRC Press,  
556 2004.
- 557 [2] A. Abbas, M. Carcasses, and J.-P. Ollivier, “Gas permeability of concrete in relation to  
558 its degree of saturation,” *Mater. Struct.*, vol. 32, no. 1, pp. 3–8, 1999.
- 559 [3] L. Basheer, J. Kropp, and D. J. Cleland, “Assessment of the durability of concrete from  
560 its permeation properties : a review,” *Constr. Build. Mater.*, vol. 15, no. 2–3, pp. 93–103,  
561 Mar. 2001.
- 562 [4] J.-P. Ollivier, J.-M. Torrenti, and M. Carcasses, *Propriétés physiques du béton et de ses*  
563 *constituants*. Hermes, Lavoisier, 2012.
- 564 [5] F. Ghasemzadeh, R. Rashetnia, D. Smyl, and M. Pour-Ghaz, “A comparison of methods  
565 to evaluate mass transport in damaged mortar,” *Cem. Concr. Compos.*, vol. 70, pp. 119–  
566 129, Jul. 2016.
- 567 [6] AFPC-AFREM, *Compte-rendu des journées techniques AFPC/AFREM. Durabilité des*  
568 *bétons, “Méthodes recommandées pour la mesure des grandeurs associées à la*  
569 *durabilité”, 11 and 12 december 1997, LMDC Toulouse / Réf. ATILH n°37864. 1997.*
- 570 [7] Norme XP P18-463, *Norme XP P18-463 - Essai pour béton durci - Essai de*  
571 *perméabilité à l’air. 1999.*
- 572 [8] V. Picandet, “Influence d’un endommagement mécanique sur la perméabilité et sur la  
573 diffusivité hydrique des bétons,” Ph.D. Thesis, Ecole Centrale de Nantes, 2001.
- 574 [9] H. E. A. Sogbossi, “Etude de l’évolution de la perméabilité du béton en fonction de son  
575 endommagement : transposition des résultats de laboratoire à la prédiction des débits de  
576 fuite sur site,” Ph.D. Thesis, Université de Toulouse, Université Toulouse III - Paul  
577 Sabatier, 2017.
- 578 [10] C. Villani, R. Loser, M. J. West, C. Di Bella, P. Lura, and W. J. Weiss, “An inter lab  
579 comparison of gas transport testing procedures : Oxygen permeability and oxygen  
580 diffusivity,” *Cem. Concr. Compos.*, vol. 53, pp. 357–366, Oct. 2014.
- 581 [11] P. C. Carman, *Flow of Gases Through Porous Media*. Academic Press, 1956.
- 582 [12] D. Hoffman, B. Singh, and J. H. Thomas III, *Handbook of vacuum science and*  
583 *technology*. Academic Press, 1997.
- 584 [13] L. J. Klinkenberg, “The permeability of porous media to liquids and gases,” *Drilling and*  
585 *production practice, American Petroleum Institute*, 01-Jan-1941.
- 586 [14] A. S. Ziarani and R. Aguilera, “Knudsen’s permeability correction for tight porous  
587 media,” *Transp. Porous Media*, vol. 91, no. 1, pp. 239–260, Jan. 2012.

- 588 [15] D. Perraton, P.- Aitcin, and A. Carles-Gibergues, “Mesure de la perméabilité aux gaz des  
589 bétons : perméabilité apparente et perméabilité intrinsèque. Partie I - Validation des  
590 concepts de Carman et de Klinkenberg dans le cas d’un BHP,” *Bull. Lab. Ponts*  
591 *Chaussées*, no. 221, May 1999.
- 592 [16] J. Verdier, “Contribution à la caractérisation de l’évolution du taux de fuite des enceintes  
593 de confinement du parc nucléaire,” Ph.D. Thesis, Université de Toulouse, Université  
594 Toulouse III-Paul Sabatier, 2001.
- 595 [17] Norme NF P18-459, *Norme NF P18-459 - Béton - Essai pour béton durci - Essai de*  
596 *porosité et de masse volumique*. 2010.
- 597 [18] V. Baroghel-Bouny *et al.*, “Méthodes d’essai N°58 : Caractéristiques microstructurales  
598 et propriétés relatives à la durabilité des bétons : Méthodes de mesure et d’essai de  
599 laboratoire,” *Tech. Méthodes Lab. Ponts Chaussées-LCPC Cerca Con Google*, 2002.
- 600 [19] H. Sogbossi, J. Verdier, and S. Multon, “Impact of reinforcement-concrete interfaces and  
601 cracking on gas transfer in concrete,” *Constr. Build. Mater.*, vol. 157, pp. 521–533, Dec.  
602 2017.
- 603 [20] V. Garnier, “Evaluation non destructive des enceintes de confinement des centrales  
604 nucléaires - Compte rendu de la Réunion plénière N°6,” ISFTTAR, Nantes, Jan. 2017.
- 605 [21] R. J. Torrent, “A two-chamber vacuum cell for measuring the coefficient of permeability  
606 to air of the concrete cover on site,” *Mater. Struct.*, vol. 25, no. 6, pp. 358–365, 1992.
- 607 [22] J.-P. Ollivier and J.-M. Torrenti, “La structure poreuse des bétons et les propriétés de  
608 transfert,” *Durabilité Bétons*, vol. 1, 2008.
- 609 [23] A. Lobet, *Influence des paramètres de composition des matériaux cimentaires sur les*  
610 *propriétés de transfert*. Ph.D. Thesis, Toulouse, INSA, 2003.
- 611 [24] J. J. Kollek, “The determination of the permeability of concrete to oxygen by the  
612 Cembureau method-a recommendation,” *Mater. Struct.*, vol. 22, no. 3, pp. 225–230,  
613 1989.
- 614 [25] C. Antón, M. A. Climent, G. de Vera, I. Sánchez, and C. Andrade, “An improved  
615 procedure for obtaining and maintaining well characterized partial water saturation states  
616 on concrete samples to be used for mass transport tests,” *Mater. Struct.*, vol. 46, no. 8,  
617 pp. 1389–1400, Nov. 2012.
- 618 [26] RILEM TC 116-PCD, “Permeability of concrete as a criterion of its durability, final  
619 report,” *Mater. Struct.*, vol. 32, no. 217, pp. 163–173, Apr. 1999.
- 620 [27] M. Carcassès, A. Abbas, J.-P. Ollivier, and J. Verdier, “An optimised preconditioning  
621 procedure for gas permeability measurement,” *Mater. Struct.*, vol. 35, no. 1, pp. 22–27,  
622 2001.
- 623 [28] S. Dushman and Research Staff of General Electric Research Laboratory, “Scientific  
624 foundations of vacuum technique,” *Am. J. Phys.*, vol. 30, no. 8, pp. 612–612, 1962.
- 625 [29] J. Verdier, M. Carcassès, and J. P. Ollivier, “Modelling of a gas flow measurement :  
626 Application to nuclear containment vessels,” *Cem. Concr. Res.*, vol. 32, no. 8, pp. 1331–  
627 1340, Aug. 2002.
- 628 [30] Y.-S. Wu, K. Pruess, and P. Persoff, “Gas Flow in Porous Media With Klinkenberg  
629 Effects,” *Transp. Porous Media*, vol. 32, no. 1, pp. 117–137, Jul. 1998.
- 630 [31] D. Gardner, “Experimental and numerical studies of the permeability of concrete,” Ph.D.  
631 Thesis, Cardiff University, 2005.
- 632 [32] G. E. Karniadakis, A. Beskok, and N. Aluru, *Microflows and Nanoflows: Fundamentals*  
633 *and Simulation*. Springer Science & Business Media, 2005.
- 634 [33] S. Roy, R. R. F. Chuang, B. A. Cruden, and M. Meyyappan, “Modeling gas flow  
635 through microchannels and nanopores,” *J. Appl. Phys.*, vol. 93, no. 8, pp. 4870–4879,  
636 Mar. 2003.

- 637 [34] J. F. O’Hanlon, *A user’s guide to vacuum technology*, 3rd edition. John Wiley & Sons,  
638 2005.
- 639 [35] N. P. Pham, A. Toumi, and A. Turatsinze, “Effect of Styrene-Butadiene Copolymer  
640 Coating on Properties of Rubberized Cement-Based Composites,” in *Strain-Hardening  
641 Cement-Based Composites*, vol. 15, V. Mechtcherine, V. Slowik, and P. Kabele, Eds.  
642 Dordrecht: Springer Netherlands, 2018, pp. 342–350.
- 643 [36] J. Verdier and M. Carcassès, “Equivalent gas permeability of concrete samples subjected  
644 to drying,” *Mag. Concr. Res.*, vol. 56, no. 4, pp. 223–230, May 2004.
- 645 [37] F. A. Florence, J. Rushing, K. E. Newsham, and T. A. Blasingame, “Improved  
646 Permeability Prediction Relations for Low Permeability Sands,” 2007.
- 647 [38] F. Cassagnabère, “Produits préfabriqués en béton filé : vers l’amélioration des  
648 performances du matériau pour mieux gérer le procédé de production,” PhD Thesis,  
649 Université de Toulouse, Université Toulouse III-Paul Sabatier, 2007.
- 650 [39] M. Binh, “Etude de la perméabilité des mortiers de ciment soumis à l’alcali réaction,”  
651 Rapport de stage de recherche, Université de Toulouse, Université Toulouse III-Paul  
652 Sabatier, 2007.
- 653 [40] P. Van den Heede, E. Gruyaert, and N. De Belie, “Transport properties of high-volume  
654 fly ash concrete: Capillary water sorption, water sorption under vacuum and gas  
655 permeability,” *Cem. Concr. Compos.*, vol. 32, no. 10, pp. 749–756, Nov. 2010.
- 656 [41] J. Castro, D. Bentz, and J. Weiss, “Effect of sample conditioning on the water absorption  
657 of concrete,” *Cem. Concr. Compos.*, vol. 33, no. 8, pp. 805–813, 2011.
- 658 [42] M. T. Van Genuchten, “A closed-form equation for predicting the hydraulic conductivity  
659 of unsaturated soils,” *Soil Sci. Soc. Am. J.*, vol. 44, no. 5, pp. 892–898, 1980.
- 660

661